Imaging Tumors with an Albumin-Binding Fab, a Novel Tumor-Targeting Agent

Mark S. Dennis,[1] Hongkui Jin,[2] Debra Dugger,[2] Renhui Yang,[2] Leanne McFarland,[3] Annie Ogasawara,[3] Simon Williams,[3] Mary J. Cole,[3] Sarajane Ross,[2] and Ralph Schwall[2]

Departments of [1]Antibody Engineering, [2]Translational Oncology, and [3]Biomedical Imaging, Genentech, Inc., South San Francisco, California

Abstract

Association with albumin as a means to improve biodistribution and tumor deposition of a Fab was investigated using AB.Fab4D5, a bifunctional molecule derived from trastuzumab (HERCEPTIN) capable of binding albumin and tumor antigen HER2 (erbB2) simultaneously. AB.Fab4D5 was compared with trastuzumab and a trastuzumab-derived Fab (Fab4D5) for the ability to target tumors overexpressing HER2 in mouse mammary tumor virus/HER2 allograft models. Biodistribution was monitored using intravital microscopy, histology, and integrated single-photon emission computed tomography/computed tomography analysis. Fab4D5 tumor deposition was characterized by rapid but transient appearance in tumor at 2 h with little retention, followed by rapid accumulation in kidney by 6 h. Trastuzumab was slow to accumulate in tumors and slow to clear from normal tissues, although significant tumor deposition was achieved by 24 h. In contrast, AB.Fab4D5 was observed at 2 h in tumor and its presence was sustained beyond 24 h similar to trastuzumab. Intravital microscopy revealed that at peak tumor accumulation, tumor cell staining by AB.Fab4D5 was more uniform than for Fab4D5 or trastuzumab. Similar tumor deposition was achieved for both AB.Fab4D5 and trastuzumab at 48 h (35.9 $\pm$ 1.8% and 38.2 $\pm$ 3.1% injected dose/g); however, AB.Fab4D5 targeted tumors more rapidly and quickly cleared from blood, leading to a lower overall normal tissue exposure. Importantly, unlike Fab4D5, AB.Fab4D5 did not accumulate in kidney, suggesting that association with albumin leads to an altered route of clearance and metabolism. Rapid targeting, excellent tumor deposition and retention, coupled with high tumor to blood ratios may make AB.Fab an exceptional molecule for imaging and cancer therapy. [Cancer Res 2007;67(1):254–61]

Introduction

Tumors present many barriers to efficient delivery of therapies. The rapid growth of tumors leads to heterogeneous vascularization, variable blood flow, and high interstitial fluid pressure that opposes convection and diffusion. Additional factors influencing immunotherapy include level of antigen expression, rate of antigen metabolism or internalization, affinity for antigen and dose of targeting agent, and its pharmacokinetics (1–3). To be therapeutically beneficial, targeted immunotherapy must be able to discriminate between tumor and normal tissue, deliver a sufficient dose to tumor, distribute evenly throughout tumor, be retained in tumor, and limit normal tissue exposure and normal organ uptake.

In addition to antibodies, many engineered immunoglobulin fragments varying in size, valency, and pharmacokinetic variables have been explored. Small antibody fragments tend to have increased vascular permeability, diffuse more rapidly into tumors, and distribute more evenly due to their lower molecular weight (4–10). They are also cleared rapidly from blood, limiting most normal tissue exposure. Due to their rapid plasma clearance, however, they tend to accumulate in kidney and deposition in tumor is often limited. In contrast, antibodies achieve relatively high concentrations in tumor despite their slow rate of diffusion and poor vascular permeability; however, they tend to distribute heterogeneously within the tumor (11). Further, their slow clearance from the body results in high normal tissue exposure (11–13).

Here, we investigate albumin as a potential delivery vehicle for immunotherapy. Known to accumulate in and be catabolized by tumors, albumin has previously been pursued as a delivery vehicle for chemotherapy (14–18). Combining this observation with immunotherapy, we explore the ability of an albumin-binding Fab (AB.Fab) to specifically target tumors. This bifunctional molecule retains the ability to bind antigen, whereas clearance from serum is greatly reduced through its constant association with albumin *in vivo* (19, 20).

HER2, an established tumor marker overexpressed in a wide variety of cancers, including 25% to 30% of breast cancers, is a prognostic indicator of long-term survival in patients (21). These tumors have been effectively treated with trastuzumab (HERCEPTIN), a humanized monoclonal antibody that recognizes the extracellular domain of HER2 (22). Using mouse mammary tumor virus (MMTV)/HER2 mouse allograft models, we compare trastuzumab with a trastuzumab-derived Fab (Fab4D5) and AB.Fab (AB.Fab4D5) for the ability to target tumors overexpressing HER2. We show that an AB.Fab rapidly targets tumors, achieves a tumor deposition comparable with that of IgG, and quickly achieves high tumor to normal tissue ratios.

Materials and Methods

All experimental procedures conformed to guiding principles of the Guide for the Care and Use of Laboratory Animals and American Physiology Society and were approved by the Institutional Animal Care and Use Committee of Genentech (South San Francisco, CA).

Production of Fab4D5, AB.Fab4D5, and AB.FabATF. Methods for producing Fab4D5 (23), AB.FabATF (formerly D3h44-L; ref. 19), and AB.Fab4D5 (20) have been described previously. An AB.Fab is constructed by adding a linker (GGGS) and an albumin-binding peptide (QRLMEDICLPRWGCLWEDDF) to either the carboxyl terminus of the heavy chain

Note: This work is dedicated to the fond memory of our friend and colleague, Ralph Schwall.

Requests for reprints: Mark S. Dennis, Antibody Engineering Department, Genentech, Inc., 1 DNA Way, MS27, South San Francisco, CA 94080. Phone: 650-225-1162; Fax: 650-225-3734; E-mail: msd@gene.com.

doi:10.1158/0008-5472.CAN-06-2531

(as with AB.Fab4D5) or light chain (as with AB.FabATF) of a Fab yielding essentially identical improvements in pharmacokinetics (19, 20).

Albumin, HER2, and tissue factor binding assays. Assays used to measure albumin binding affinity have been described previously (19, 20). Pharmacokinetics of trastuzumab, AB.Fab4D5, and Fab4D5 in mouse serum were monitored using a HER2-binding ELISA (20). Serum concentrations of anti–tissue factor Fab (AB.FabATF) were assayed using a tissue factor ELISA (19).

Trastuzumab competition ELISA. Direct competition to block trastuzumab binding to immobilized HER2 extracellular domain ($HER2_{ecd}$) was used to verify functional antigen binding of Fab4D5 and AB.Fab4D5 in the presence or absence of albumin. Immunosorbant microtiter plates were coated with 1 μg/mL $HER2_{ecd}$ overnight at 4°C, washed, and blocked with Casein Blocker (Pierce Biotechnology, Rockford, IL) for 1 h at 25°C. Serially diluted serum samples were added to wells along with 100 ng/mL trastuzumab in 1% ovalbumin in PBS and 0.05% Tween 20 with or without 500 nmol/L rabbit albumin for 2 h at 25°C. Plates were washed and bound trastuzumab was detected using goat anti-human Fc·horseradish peroxidase (HRP; Jackson Laboratory, Bar Harbor, ME). Bound HRP was assayed with tetramethylbenzidine/H_2O_2. The reaction was quenched using 1 mol/L phosphoric acid and monitored at 450 nm. A four-variable fit was used to fit data and estimate IC_{50}.

Binding to albumin and HER2 simultaneously. Simultaneous binding to $HER2_{ecd}$ and albumin was monitored by the ability to bridge the interaction between immobilized rabbit albumin and biotinylated $HER2_{ecd}$. $HER2_{ecd}$ was biotinylated using a 4-fold molar excess of NHS-LS-biotin (Pierce Biotechnology). Plates were coated with 10 μg/mL rabbit albumin (Sigma, St. Louis, MO) overnight at 4°C. Wells blocked with 1% ovalbumin in PBS were incubated with 2 μmol/L AB.Fab4D5 or Fab4D5 for 1 h, washed, and a titration of biotinylated $HER2_{ecd}$ was added for 1.5 h. Wells were washed, and bound biotinylated $HER2_{ecd}$ was detected using streptavidin-HRP (SouthernBiotech, Birmingham, AL). Bound HRP was assayed as above.

Mouse allograft models. MMTV/HER2 transgenic mice develop mammary tumors expressing elevated levels of human HER2 with a latency of ~4 to 6 months. These tumors are readily transplanted into wild-type murine hosts. For these studies, two mammary tumors derived from MMTV/HER2 transgenic FVB mice were used: MMTV/HER2 Founder 5 (designated Fo5; ref. 24) and MMTV/HER2 F2-1282 (designated F2-1282).

The Fo5 mammary tumor line was maintained through serial passaging via surgical implant of 2-mm^3 sections of tumor into the second right mammary fat pad of wild-type FVB mice. Fo5 expresses >1,000,000 copies of human HER2 per cell and does not respond to trastuzumab (no change in growth rate versus controls when 30 mg/kg trastuzumab is administered twice weekly for 4 weeks). For this study, the Fo5 mammary tumor was surgically transplanted into the second mammary fat pad of beige-nude-xid mice (Charles River Labs, Hollister, CA) as 2-mm^3 sections. The tumor was serially passaged 13 times in wild-type FVB mice before implant into beige-nude-xid mice. Transplanted mice were randomized to distribute comparably sized tumors into each group. Mean tumor volumes for each treatment group ranged between 150 and 220 mm^3. Individual tumor volumes were obtained from measurements of tumor length and width in millimeter using a digital caliper and calculated as follows: tumor volume (mm^3) = (longer diameter × shorter $diameter^2$) × 0.5.

For intravital microscopy, the F2-1282 mammary tumor line was used. F2-1282 is the offspring of an F_1 transgenic animal from the MMTV/HER2 Fo2936-3 line. This tumor was maintained through serial passaging via surgical implant of 2-mm^3 sections into the second right mammary fat pad of wild-type FVB mice. F2-1282 expresses >1,000,000 copies of human HER2 per cell and is responsive to trastuzumab therapy (100% of F2-1282 tumor-bearing animals exhibit complete tumor regression with 30 mg/kg trastuzumab administered weekly for 3 weeks).

Tumor staining. Trastuzumab, AB.Fab4D5, AB.FabATF, and Fab4D5 were labeled with a fluorescent cyanine compound, Cy3, using Amersham Cy3 monofunctional dye kit (Amersham Biosciences, Piscataway, NJ) according to kit protocol. Molar ratios of Cy3/protein were 7.0, 4.8, 5.6, and 4.0, respectively. To compare intensity and duration of Cy3 signal across study groups, administered dose was normalized to Cy3 concentration. Protein doses ranged from 1.35 to 2.4 mg/kg and Cy3 equivalents ranged from 189 to 224 units. Mice bearing 150 to 220 mm^3 Fo5 tumors were dosed (nine mice per group) as follows: AB.Fab4D5 (40 μg × 4.8 dye/AB.Fab = 192 units/dose), Fab4D5 (48 μg × 4 dye/Fab = 192 units/dose), AB.FabATF (40 μg × 5.6 dye/AB.Fab = 224 units/dose), and trastuzumab (27 μg × 7 dye/IgG = 189 units/dose). Dosing solutions (0.1–0.11 mL) were administered by i.v. tail vein injection as a single bolus at time 0.

At 2, 24, and 48 h postinjection, three mice were anesthetized per group and a blood sample was collected for pharmacokinetic analysis. Peripheral vascular perfusion was done by flushing 0.9% saline through the left ventricle of the heart. Tumors were harvested, stored in 20% sucrose at 4°C for 1 h, and embedded into optimum cutting temperature (OCT) mounting medium at −70°C. Frozen tumor sections (6 μm) were cut using a Leica cryostat and mounted with Vectashield mounting media with DAPI nuclear stain (Vector Labs, Burlingame, CA) to counterstain nuclei. Two sections at 240- and 430-μm depth into each tumor were examined using a Nikon TE300 fluorescent microscope. Images using 10-, 20-, and 30-s exposures were captured using Spot Basic v3.5.2. Final images were generated using Adobe PhotoShop.

Single-photon emission computed tomography/computed tomography imaging. Fab4D5, AB.Fab4D5, and trastuzumab (10 mg/mL in PBS, 2.5 mmol/L EDTA) were conjugated with 5 mg/ml of 1,4,7,10-tetraazacylododecane *N,N′,N″,N‴*-tetraacetic acid mono-(*N*-hydroxysuccinimidyl) ester (DOTA-NHS; Macrocyclics, Inc., Dallas, TX) in *N-N′*-dimethylacetamide at a 5:1 molar ratio at 30°C for 1 h. Electrospray mass spectrometry revealed peaks for each conjugate with increasing integral numbers of DOTA substituents allowing conjugation distribution to be directly determined. Metal ions present in DOTA remain bound during mass spectrometry, enabling the number of empty binding sites per molecule to be determined. Conjugations typically resulted in a median two DOTA per protein.

$Indium^{111}$ chloride (MDS Nordion, Vancouver, BC) was mixed at 50 μL/mL of DOTA conjugate in 0.3 mol/L ammonium acetate at 25°C for 1 h. Reactions were quenched with 2 mmol/L diethylenetriaminepentaacetic acid and desalted using NAP-5 columns (GE-Amersham, Piscataway, NJ). Samples typically contained ~2 mCi/mg protein.

Mice bearing 150 to 220 mm^3 Fo5 tumors were anesthetized with isoflurane and placed prone on the animal bed of an X-SPECT (Gamma Medica, Northridge, CA). Body temperature was maintained at 37°C with warm airflow under feedback control. Therapeutic doses of [^{111}In]DOTA-labeled conjugates (4 mg/kg and 300–500 μCi) were injected via tail vein. Single-photon emission computed tomography (SPECT) and computed tomography (CT) images were acquired consecutively in the same dual gamma camera X-SPECT at 1, 6, 24, and 48 h postinjection. Each data set consisted of 64 × 30-s SPECT projections. Images were reconstructed using an ordered subsets EM algorithm. After the final image, tissues were harvested and weighed, and radioactivity was measured in a gamma-well counter for comparison with image-based measurements. Regions of interest were defined using CT volumes to compute region of interest intensities for corresponding SPECT images. SPECT images were scaled according to a known reference standard. A comparison of *ex vivo* signals with *in vivo* image intensities was used to determine empirical recovery coefficients for each tissue allowing qualitative localization of [^{111}In]DOTA-conjugated Fab4D5, AB.Fab4D5, and trastuzumab at each time point.

Intravital microscopy. Female athymic nude mice (The Jackson Laboratory) were acclimated to animal housing for at least 1 week before surgery. Mice were anesthetized by i.p. injection of ketamine 80 mg/kg (Aveco Co., Inc., Fort Dodge, IA) and xylazine 10 mg/kg (Rugby Laboratories, Inc., Rockville Center, NY). The surgery procedure reported by Leunig et al. (24) was used with modification. After cleaning the dorsal lumbar and thoracic area with antimicrobial Betadine solution and alcohol, two symmetrical titanium frames (Research Instruments, Inc., Durham, NC)—mirror images of each other—were used to sandwich an extended double layer of skin. One layer was removed in a circular area ~15 mm in diameter; the remaining layer consisting of epidermis, s.c. tissue, and striated muscle was covered with a glass overslip incorporated into one of the frames. Two days after implantation of the dorsal chamber, the overslip

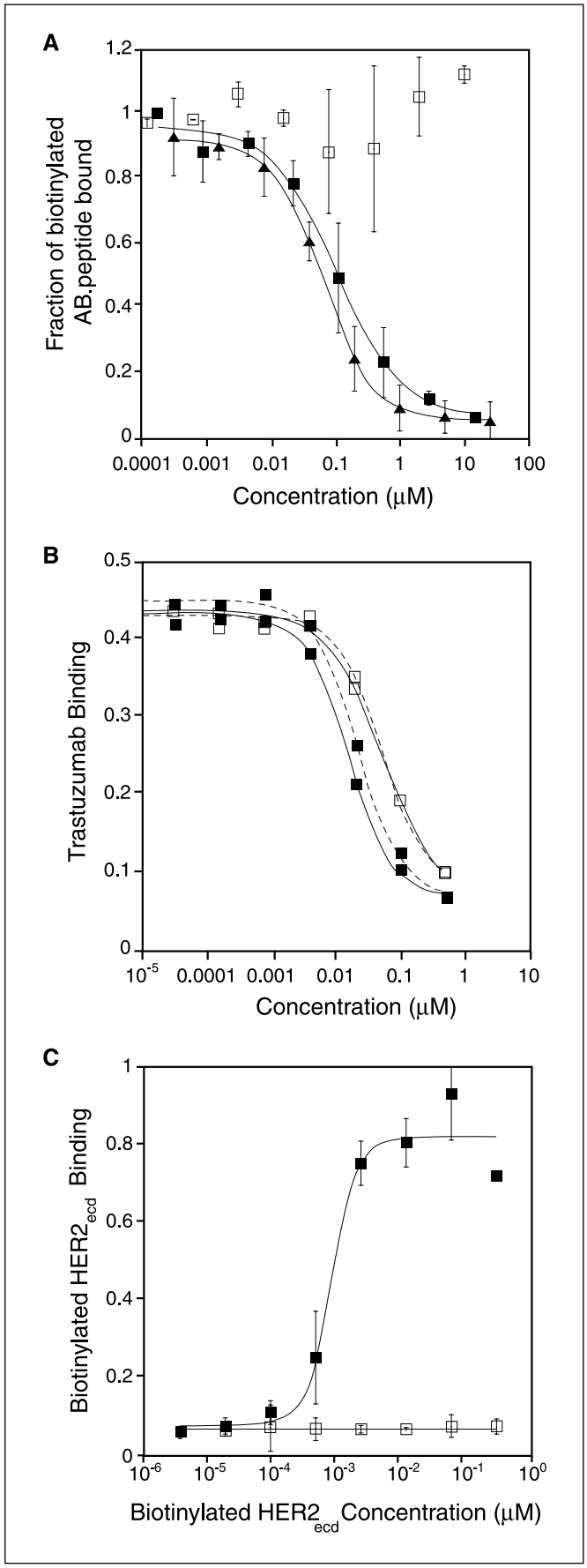

was removed and a 1-mm-diameter piece of F2-1282 tumor was implanted onto the fascia at the center of the chamber. A new overslip was placed on the chamber. Tumor growth was monitored at least twice weekly. When tumors reached 3 to 4 mm in diameter, animals were randomized to receive i.v. injection of FITC-trastuzumab 10 mg/kg (n = 4), FITC-Fab4D5 20 mg/kg (n = 5), or FITC-AB.Fab4D5 20 mg/kg (n = 5). Molar ratios of FITC/protein were 3.2, 1.7, and 1.65, respectively. Using a Nipkow spinning disc confocal unit (Yokogawa Corporation of America, Newman, GA, model CSU 10) equipped with an intensified charge coupled device camera (Stanford Photonics, Inc., Palo Alto, CA model XR/Mega-10) and installed on a standard upright microscope (Nikon Instruments, Inc., Melville, NY, model Eclipse E800), tumors were imaged at 2 h postinjection for FITC-Fab4D5 and 24 h for FITC-AB.Fab4D5 and FITC-trastuzumab. Times were selected from an earlier time course study that showed maximal uptake of fluorescence in tumor cells at these times.

At necropsy, tumor tissue from dorsal-skin chamber tumors was embedded in OCT compound (Sakura Fineteck, Torrance, CA) and frozen at −80°C. Cryostat sections (5 μmol/L) were cut through tumor tissue and slides were allowed to dry at 25°C for 2 to 4 h. Slides were stored at −80°C until ready for staining and protected from light for all manipulations. Frozen sections were fixed in ice-cold methanol for 10 min and washed twice in PBS. Serum-Free Protein Block (DakoCytomation, Carpinteria, CA) was applied to each slide in a humidified chamber for 10 min. To visualize endothelial cells, 150 μL of rat anti-mouse CD31 (BD Bioscience PharMingen, San Jose, CA) at 10 μg/mL in protein blocking solution were applied to each slide for 2 h at 25°C in a humidified chamber. Slides were rinsed twice in PBS and 150 μL of Cy3-conjugated, affinity-purified goat anti-Rat IgG (Jackson ImmunoResearch Laboratories, Inc., West Grove, PA) were diluted 1:400 in DAKO blocking solution and applied for 30 min. Slides were washed twice with PBS and mounted with Vectashield mounting medium with DAPI nuclear stain (Vector Labs, Burlingame, CA). Slides were kept protected from light at 4°C until visualized by fluorescence microscopy.

Histologic quantification of vascular area, penetrated area, and total area was done using Image J software.

Pharmacokinetic analysis. BALB-c mice (Charles River Labs, Hollister, CA), weighing between 17 and 20 g, were given 5 mg/kg trastuzumab, Fab4D5, or AB.Fab4D5 (n = 9 mice per group) i.v. bolus via tail vein. Over 14 days, serum was collected from three mice per time point by retro-orbital bleed or cardiac aspiration. Serum samples were assayed as previously described (20).

Results

Characterization of AB.Fab4D5. An albumin affinity column was used during AB.Fab4D5 purification to ensure a properly folded albumin-binding peptide. Albumin binding was shown by the ability of AB.Fab4D5 to displace a biotinylated albumin-binding peptide (SA06b) from binding to rabbit albumin. AB.Fab4D5 and unbiotinylated albumin-binding peptide, SA06, displaced SA06b to a similar extent, whereas Fab4D5 had no effect in this assay (Fig. 1*A*). Binding of AB.Fab4D5 to $HER2_{ecd}$ was comparable with Fab4D5 and was unaffected by the presence of rabbit albumin (Fig. 1*B*). IC_{50} values obtained for displacement of trastuzumab, a bivalent IgG, binding to $HER2_{ecd}$ merely represent an upper limit to the affinity of Fab4D5 and AB.Fab4D5. Affinity of Fab4D5 for $HER2_{ecd}$ was previously

Figure 1. Properties of AB.Fab4D5. *A,* the ability of Fab4D5 (□), AB.Fab4D5 (■), and SA06 (△; ref. 19) to block binding of biotinylated albumin-binding peptide to immobilized rabbit albumin. The IC_{50} values obtained for AB.Fab4D5 and SA06 were 107 and 65 nmol/L, respectively. *B,* the ability of Fab4D5 (□) and AB.Fab4D5 (■) to block binding of trastuzumab to immobilized $HER2_{ecd}$ is not affected by albumin. IC_{50} values in the presence (*dashed line*) or absence (*solid line*) of 0.5 μmol/L rabbit albumin were 22 and 15 nmol/L for AB.Fab4D5 and 51 and 53 nmol/L for Fab4D5, respectively. *C,* the ability of Fab4D5 (□) and AB.Fab4D5 (■) to simultaneously bind immobilized albumin and biotinylated $HER2_{ecd}$ was monitored as a function of increasing concentrations of biotinylated $HER2_{ecd}$.

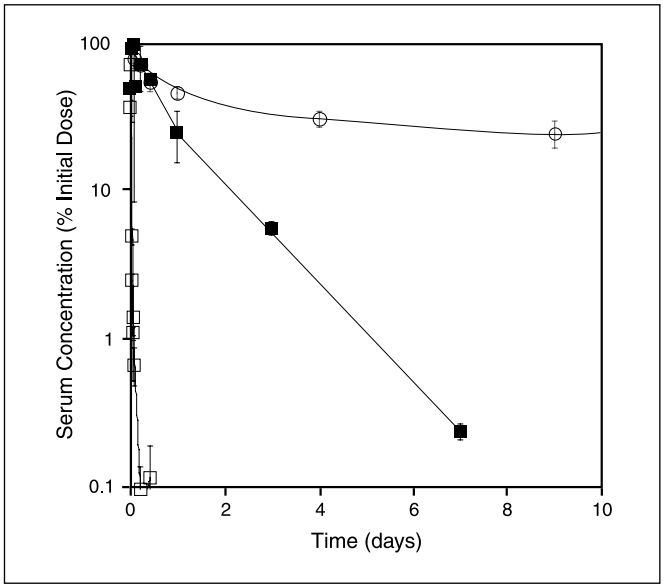

Figure 2. Elimination profiles of Fab4D5, AB.Fab4D5, and trastuzumab in mouse. The serum concentration of Fab4D5 (□), AB.Fab4D5 (■), and trastuzumab (○) were monitored in mouse over a 2-week period as described in Materials and Methods.

reported as 0.1 nmol/L (22, 25). These results, however, suggest that AB.Fab4D5 binds $HER2_{ecd}$ comparable with Fab4D5, and binding is not dramatically affected by albumin/AB.Fab4D5 complex formation. Ability of AB.Fab4D5 to bind $HER2_{ecd}$ and albumin simultaneously was shown by binding AB.Fab4D5 to immobilized albumin followed by detection with biotinylated $HER2_{ecd}$ (Fig. 1*C*). Fab4D5 is unable to generate a signal in this assay; however, AB.Fab4D5 acts as a bifunctional fusion protein able to bind both albumin and $HER2_{ecd}$ simultaneously.

Elimination profiles for Fab4D5, AB.Fab4D5, and trastuzumab in mouse are shown in Fig. 2.

Histologic assessment of tumor targeting. The relative ability of AB.Fab4D5, Fab4D5, and trastuzumab to target HER2-overexpressing tumors was initially assessed using a mammary tumor derived from an MMTV/HER2 transgenic FVB mouse (26) that does not respond to trastuzumab (Fo5). Dose of the Cy3-conjugated proteins was normalized to fluorescence and administered i.v. Tumors were harvested at 2, 24, or 48 h; sectioned; and examined for the presence of targeting molecules (Fig. 3). Strong initial staining of all tumor cells at 2 h postinjection was observed with Fab4D5 followed by predominantly weak, membranous staining at 24 h and a complete lack of signal at 48 h (Fig. 3). In contrast, Fo5 tumors treated with AB.Fab4D5 displayed robust membranous staining distributed throughout the tumor at 2 and 24 h after i.v. injection. Staining intensity of AB.Fab4D5 began to diminish by 48 h, although in all three animals, its presence was still detected in a majority of cells throughout the tumor. Poor tumor penetration by trastuzumab was noted at 2 h postinjection, with cells in the outer lobes of tumor displaying a robust, membranous Cy3-signal and cells deeper in tumor remaining unlabeled. By 24 h, trastuzumab had begun to penetrate deeper into Fo5 tumors with half of the cells displaying a robust staining and half staining weakly. At 48 h, trastuzumab penetration was variable, with two tumors demonstrating a predominance of membranous staining only in outer lobes of the tumor. The third tumor showed greater penetration by trastuzumab after 48 h, with ~80% of tumor cells exhibiting a strong membranous staining.

Thus, although Fab4D5 and AB.Fab4D5 prominently stain tumor initially, at later time points (24 and 48 h) when

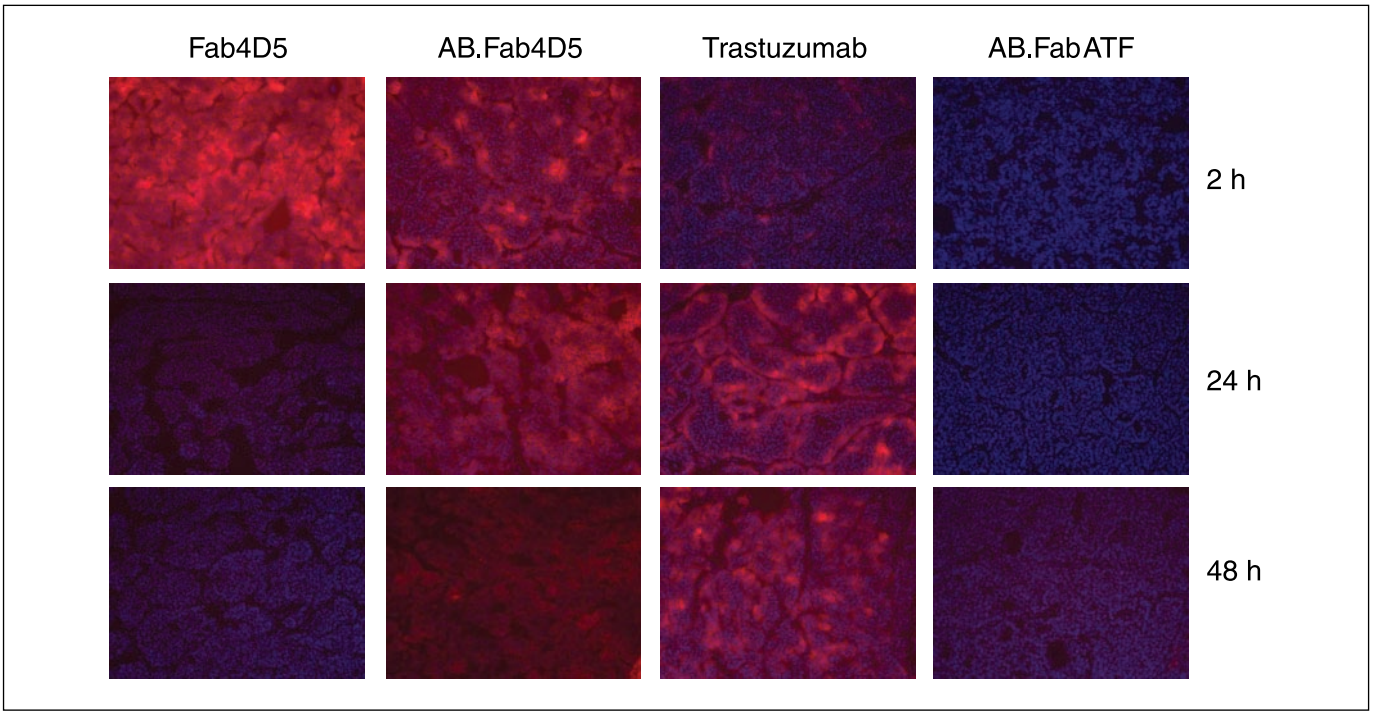

Figure 3. *In vivo* targeting of Fo5 tumors by Cy3-conjugated Fab4D5, AB.Fab4D5, trastuzumab, and AB.FabATF. Following i.v. administration of Cy3-conjugated Fab4D5, AB.Fab4D5, trastuzumab, or AB.FabATF into mice bearing Fo5 tumors, tumors were harvested at 2, 24, or 48 h, and sectioned (see Materials and Methods). Fluorescence intensity is indicative of the concentration of Cy3 conjugate present in tumor at the indicated time of harvest.

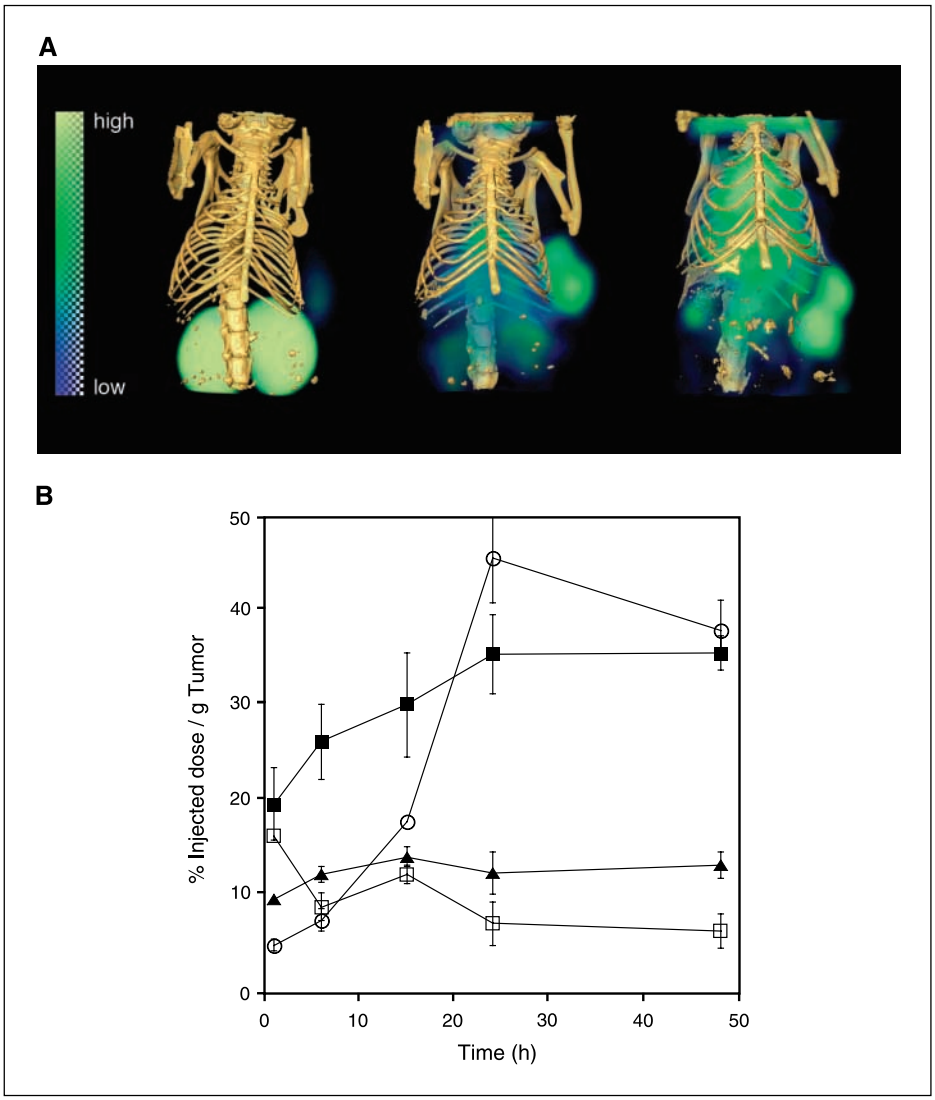

Figure 4. Biodistribution of [^{111}In]DOTA-conjugated Fab4D5, AB.Fab4D5, and trastuzumab as a function of time determined using SPECT/CT imaging. *A,* SPECT/CT fusion images depicting biodistribution of Fab4D5, AB.Fab4D5, and trastuzumab at 18 h. Consecutive ^{111}In SPECT (*color scale*) and X-ray CT (*ivory*) tomographic images were acquired. Images were coregistered by geometric transformation and fused with Analyze (AnalyzeDirect, Inc., Lenexa, KS) and then rendered to make the composite images (Amira, Mercury Computer Systems, Inc., Richmond, TX). Visualization was further aided by studying original data as movies in three dimensions. Fab4D5 (*left*) shows classic kidney clearance; trastuzumab (*right*) shows pronounced tumor uptake and substantial remaining blood pool. AB.Fab4D5 (*middle*) distribution was more like trastuzumab than Fab4D5, with pronounced tumor uptake, some residual blood pool, and only low-level kidney uptake. *B,* concentration (percent injected dose per gram of tumor) of Fab4D5, AB.Fab4D5, and trastuzumab over time was compared using SPECT/CT imaging. Over a period of 48 h, mice (n = 5 or 6 per group) were imaged on five consecutive occasions with combined SPECT/CT imaging as described in Materials and Methods. Tumor SPECT intensities of Fab4D5 (□), AB.Fab4D5 (■), trastuzumab (○), and AB.FabATF (▲) were converted to percent injected dose per gram by reference to a standard of known activity included in each image.

trastuzumab begins to appear, Fab4D5 is no longer present in tumor. In contrast, AB.Fab4D5 maintains a prominent staining pattern and is effectively retained in tumor similar to trastuzumab. A negative control AB.Fab, AB.FabATF, does not recognize any mouse antigen and did not stain tumor at any time during the experiment, demonstrating that targeting by AB.Fab4D5 is antigen dependent.

Serum samples taken during the experiment were used to assess pharmacokinetic profiles of Cy3-conjugated trastuzumab, Fab4D5, AB.Fab4D5, and AB.FabATF in mouse. Similar profiles to that previously reported in mouse were observed (19, 20). Association with albumin by either AB.Fab (AB.Fab4D5 or AB.FabATF) leads to a dramatic decrease in clearance relative to Fab4D5.

Quantitative determination of tumor targeting. To measure tumor deposition, mice bearing Fo5 tumors were injected i.v. with Fab4D5, AB.Fab4D5, AB.FabATF, and trastuzumab conjugated with DOTA and radiolabeled with ^{111}In. Their localization at 18 h is shown in Fig. 4*A*. Fab4D5 is found almost entirely in kidney, whereas both trastuzumab and AB.Fab4D5 are found both in circulation and prominently in tumor. Images taken a different time points were used to generate data in Fig. 4*B*. They revealed an early and transient appearance of Fab4D5 in tumor followed by rapid accumulation in kidney, whereas trastuzumab showed slow and progressive accumulation into tumor tissue. AB.Fab4D5 targeted tumor much more rapidly than trastuzumab and resulted in a final concentration in tumor comparable with that of trastuzumab. Tumor deposition of AB.Fab4D5 and trastuzumab was unchanged from 48 to 72 h (not shown). Accumulation of AB.Fab4D5 was greatest in tumor with relatively little normal tissue distribution (Fig. 4*A*).

Intravital microscopy. Distribution of Fab4D5, AB.Fab4D5, and trastuzumab within tumor was monitored by intravital microscopy. Mice bearing F2-1282 tumors were fit with a window over the tumor site. Upon i.v. injection, epifluorescence microscopy of tumor enabled real-time visualization of FITC-conjugated molecules circulating through tumor tissue (Fig. 5*A*). At peak staining, tumors were harvested, sectioned, and localization of targeting molecules was determined. The rate of tumor localization and penetration was similar to that observed for Cy3-conjugated molecules. The degree to which each molecule could penetrate the smallest cluster of tumor cells was observed with higher magnification (Fig. 5*B*).

Both intravital microscopy (Fig. 5*A*) and histologic imaging (Fig. 5*B*) reveal that trastuzumab only penetrated three to four cell layers into these packets of tumor cells. Quantitative analysis of

histologic sections revealed that the penetrated area (*green area*) of Fab4D5 and AB.Fab4D5 was significantly larger than that of trastuzumab ($P < 0.01$) and penetration of AB.Fab4D5 was better than that of Fab4D5 ($P < 0.05$). There was little difference in the total tumor area (*blue area*) among the three molecules (Fig. 5*C*). Therefore, the ratio of penetrated area to total area was significantly higher for Fab4D5 and AB.Fab4D5 compared with trastuzumab ($P < 0.01$) with a higher ratio for AB.Fab4D5 than Fab4D5 ($P < 0.05$). Preliminary studies using Fo5 have yielded similar images to F2-1282 tumors (data not shown).

Discussion

Efficient, specific, and uniform delivery of immunotherapies to tumor while minimizing normal tissue exposure remains a challenging problem despite identification of many highly specific tumor markers. Small immunoglobulin fragments have been explored in an effort to enhance tumor delivery and penetration yet reduce overall exposure to normal tissue; however, the tumor concentrations that these agents achieve are often low, and accumulation in kidney is high as they are rapidly cleared from blood.

In this study, we compared tumor-targeting properties of trastuzumab with an AB.Fab and Fab derived from trastuzumab; all bind to the same site on HER2 with similar affinity. The Fo5 allograft model is resistant to the growth-suppression properties of trastuzumab (26); however, all of these molecules bind Fo5 tumor cells expressing HER2 and can be internalized (data not shown).

As a bifunctional molecule, an AB.Fab retains the ability to bind antigen but is also capable of binding albumin (19, 20). In fact, albumin binding does not seem to impede binding of antigen as its presence did not alter AB.Fab4D5 binding to $HER2_{ecd}$ and both albumin and HER2 could be bound simultaneously (Fig. 1).

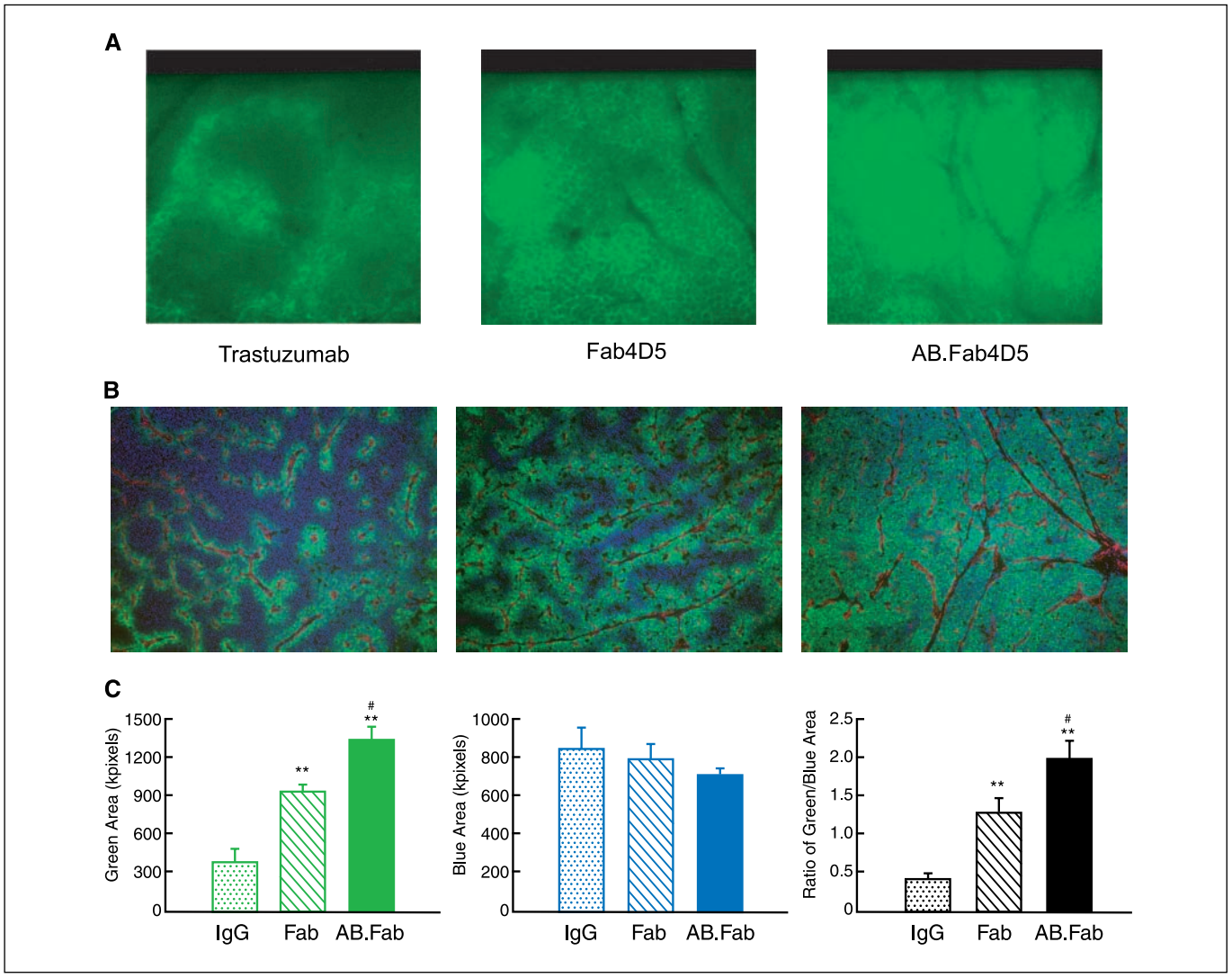

Figure 5. Assessment of tumor penetration using intravital microscopy. Tumor penetration was assessed at maximum tumor accumulation. FITC-Fab4D5 was assessed at 2 h, whereas FITC-AB.Fab4D5 and FITC-trastuzumab were assessed at 24 h postinjection. *A,* representative intravital microscopy images were recorded using confocal laser scanning microscopy at ×200 magnification. *B,* microscopic images of F2-1282 tumor tissue. Injected trastuzumab, Fab4D5, or AB.Fab4D5 conjugated with FITC (*green*) was detected over tumor tissue and displayed a membranous staining pattern. Vasculature was visualized with an anti-mouse CD31 detected with a Cy3-conjugated secondary antibody (*red*). All tissues were counterstained with DAPI (*blue*) to detect nuclei. *C,* quantitative analysis using Image J software for measurement of penetrated area (*green area*), total area (*blue area*), and their ratio. *, $P < 0.05$; **, $P < 0.01$, compared with trastuzumab; #, $P < 0.05$ compared with Fab4D5. Trastuzumab, FITC-trastuzumab ($n = 4$ mice); Fab4D5, FITC-Fab4D5 ($n = 5$ mice); AB.Fab, FITC-AB.Fab4D5 ($n = 5$ mice).

Further, *in vivo* AB.Fab4D5 showed improved pharmacokinetics relative to Fab4D5 and more effectively localized to tumors overexpressing HER2 (Figs. 2–5). AB.FabATF did not localize to tumors (Figs. 3 and 4*B*), supporting this antigen-dependent localization.

The rate of accumulation in tumor allografts was monitored in three different experiments using fluorescently labeled and radiolabeled Fab4D5, AB.Fab4D5, and trastuzumab (Figs. 3–5). Although only representative time points are presented, observations for each molecule were consistent across experiments.

In each experiment, Fab4D5 showed excellent tumor penetration by 2 h followed by rapid clearance from both serum and tumor by 24 and 48 h (Figs. 2–5). High serum concentrations of small targeting immunoglobulin molecules like Fab4D5 facilitate diffusion into tumor, but as serum concentration drops due to rapid clearance, the concentration gradient reverses and these agents diffuse back out of the tumor (27). Lack of retention in tumor by Fab4D5 suggests that it bound only transiently to the tumor surface and was not effectively internalized during its residence. Passive internalization and recycling of HER2 back to the cell surface has been previously observed (28, 29) and may account for this temporary sequestration of Fab4D5 in the tumor.

Nearly 24 h passed before significant levels of trastuzumab were observed in tumor; at the same time, its serum concentration decreased by only ~50% (Fig. 2). Slow tumor accumulation was accompanied by poor tumor penetration, with deeper penetration beyond the outer lobes of the tumor only apparent after 24 h (Figs. 3 and 5). In contrast, AB.Fab4D5 accumulated rapidly in tumors, reaching similar levels to Fab4D5 by 2 h; however, whereas Fab4D5 redistributed to kidney, AB.Fab4D5 continued to accumulate in tumor, reaching levels similar to trastuzumab (Figs. 3 and 4). AB.Fab4D5 retention suggests that a critical residence time in tumor is required for internalization and metabolism to enable permanent, rather than transient, tumor localization.

Rapid accumulation and retention in tumors coupled with an intermediate rate of clearance from serum resulted in very favorable tumor to normal tissue ratios for AB.Fab4D5 (Figs. 2 and 4). At 24 h, both tumor and serum concentrations of AB.Fab4D5 and trastuzumab were similar, however, serum concentrations of AB.Fab4D5 decreased rapidly relative to trastuzumab, resulting in lower normal tissue exposure (Figs. 2 and 4). Although small immunoglobulin fragments like scFv, diabodies, Fab, and $F(ab')_2$ have previously been observed to transiently provide good tumor to normal ratios similar or even greater to that achieved for AB.Fab4D5, none of these other agents to date have shown the ability to achieve a concentration in tumor comparable with an IgG (8, 9, 30–34). Efficient delivery of AB.Fab4D5 complemented by low backgrounds relative to trastuzumab is evident in Fig. 4.

Combination SPECT/CT imaging was used as a direct way to quantify tumor deposition. Because the label used for monitoring a targeting molecule *in vivo* can affect absolute concentration and residence time observed in different tissues, ^{111}In was used to avoid dehalogenation losses associated with traditional ^{125}I labeling chemistries (35, 36). Tumor deposition achieved by AB.Fab4D5 between 24 and 48 h was comparable with that achieved by trastuzumab and far exceeded that for Fab4D5 (Fig. 4*B*). The apparent decrease in Cy3-AB.Fab4D5 staining at 48 h (Fig. 3) relative to the stable deposition of [^{111}In]AB.Fab4D5 (Fig. 4*B*) is attributed to the nonresidualizing nature of the Cy3 label. Equivalent tumor deposition of [^{111}In]AB.Fab4D5 and [^{111}In]trastuzumab was observed at 72 h (not shown). Real-time monitoring *in vivo* precluded organ perfusion before measurement; thus, some background is expected due to the presence of blood in various tissues, such as heart, and must be considered. Our biodistribution and tumor deposition results obtained with Fab4D5 and trastuzumab compare favorably with those previously reported by others (32, 35–39). Unlike Fab4D5, AB.Fab4D5 attained a similar overall concentration to trastuzumab in tumor (Figs. 3 and 4); appearance in tumor along with clearance from normal tissues and blood is rapid, resulting in superior tumor to normal tissue ratios.

Size has been directly linked to the ability of a targeting agent to penetrate tissue. Smaller agents penetrate to depths of 8 to 10 cell layers, whereas intact antibodies tend to localize immediately adjacent to blood vessels and are less evenly distributed throughout tumor (11, 40). Using intravital microscopy, we examined tumor distribution of Fab4D5, AB.Fab4D5, and trastuzumab at their peak of tumor accumulation (Fig. 5). Results obtained with Fab4D5 and trastuzumab agree with those obtained by others using different tumor models. Deep and even penetration of Fab4D5 and AB.Fab4D5 compared with limited penetration and distribution of trastuzumab. Penetration by AB.Fab4D5 was somewhat superior to that of Fab4D5 and may stem from the longer half-life and increased residence time in tumor, allowing AB.Fab4D5 to diffuse a greater distance. For instance, estimates suggest that it takes days for an IgG to travel 1 mm (or 1 h to travel 100 μm) in a tumor (2).

Irregular blood flow in tumors contributes to heterogeneous delivery and biodistribution, thus complicating effectiveness of various therapies. To reach tumor, systemically delivered agents must cross the vascular barrier and move through the interstital space by diffusion or convection (2). Efficient delivery, and even distribution of AB.Fab4D5, suggests that it has distinct advantages relative to Fab4D5 or trastuzumab. Although it is tempting to speculate that AB.Fab4D5 offers a size advantage relative to trastuzumab, the high concentration of albumin *in vivo* should cause AB.Fab4D5 to remain bound to albumin, making the apparent molecular weight of AB.Fab4D5 closer to that of trastuzumab (68 + 52 = 120 versus 150 kDa) than that of Fab4D5 (52 versus 50 kDa). Although the collagen content of a tumor affects diffusion of macromolecules in a size-dependent fashion—particularly in the range of 68 to 150 kDa (2)—the pore size in the extracellular matrix is organized by albumin to form a regularly spaced lattice (41). Thus, the shape and slightly reduced size of the albumin/AB.Fab4D5 complex may allow preferential diffusion relative to full-length IgG.

Other mechanisms caused by association with albumin may also facilitate tumor delivery of AB.Fab4D5. Based on an observation that tumors catabolize excessive quantities of albumin (14, 15), several attempts to use albumin as a carrier for chemotherapeutic agents have been reported (16–18). In addition, Abraxane, which uses albumin to formulate and solubilize Taxol, is reported to have better biodistribution properties and reduced toxicity relative to other Taxol formulations (42).

Albumin is ubiquitously distributed in high concentrations throughout the body and methods that facilitate biodistribution, diffusion, and the ability to cross endothelial barriers have been reported. For example, numerous vascular receptors have been reported to interact with albumin and facilitate its transport across endothelium (43–45). In fact, transport of myeloperoxidase across

the endothelium is enhanced through its association with albumin and is an important means of delivering myeloperoxidase to the subendothelial space (46).

Alternatively, the size of AB.Fab4D5, either bound or unbound to albumin, combined with its pharmacokinetics may just strike an optimum balance to enable effective tumor targeting. Whatever the mechanism, favorable tumor-targeting properties of AB.Fab4D5 make it an exceptional molecule for imaging and therapy and are worthy of further investigation.

Acknowledgments

Received 7/10/2006; revised 8/31/2006; accepted 10/25/2006.

The costs of publication of this article were defrayed in part by the payment of page charges. This article must therefore be hereby marked *advertisement* in accordance with 18 U.S.C. Section 1734 solely to indicate this fact.

We thank Francisco Valles for fermentation; Paul McDonald for purification of Fab4D5 and AB.Fab4D5; Greg Bennett, Elaine Mai, and Bao-Tran Truong for assay of pharmacokinetic samples; Nicholas Van Bruggen, Joe Kowalski, and Alvin Gogineni for imaging help; Wai Lee Wong, Min Zhang, and Allen Nyguen for assays; Janie Pena for preparing the figures; and Gail Cobern and Gail Phillips for their review of the manuscript and helpful suggestions.

References

1. Graff CP, Wittrup KD. Theoretical analysis of antibody targeting of tumor spheroids: importance of dosage for penetration and affinity for retention. Cancer Res 2003;63:1288–96.
2. Jain RK. Delivery of molecular medicine to solid tumors: lessons from *in vivo* imaging of gene expression and function. J Control Release 2001;74:7–25.
3. Zuckier LS, Berkowitz EZ, Sattenberg RJ, Zhao QH, Deng HF, Scharff MD. Influence of affinity and antigen density on antibody localization in a modifiable tumor targeting model. Cancer Res 2000;60:7008–13.
4. Adams GP, Schier R. Generating improved single-chain Fv molecules for tumor targeting. J Immunol Methods 1999;231:249–60.
5. Colcher D, Goel A, Pavlinkova G, Beresford G, Booth B, Hudson PJ. Effects of genetic engineering on the therapy and pharmacokinetics of antibodies. Q J Nucl Med 1999;43:132–9.
6. Kashmiri SVS. Multivalent single-chain antibodies for radioimaging of tumors. J Nucl Med 2001;42:1528–9.
7. Li Q, Hudson W, Wang D, Berven E, Uckum FM, Kersey JH. Pharmacokinetics and biodistribution of radioimmunoconjugates of anti-CD19 antibody and single-chain Fv for treatment of human B-cell malignancy. Cancer Immunol Immunother 1998;47:121–30.
8. Milenic DE, Yokota T, Filpula DR, et al. Construction, binding properties, metabolism, and tumor targeting of a single-chain Fv derived from the pancarcinoma monoclonal antibody CC49. Cancer Res 1991;51:6363–71.
9. Rowlinson-Busza G, Deonarain MP, Epenetos AA. Comparison of intact monoclonal antibody, its F(ab')2 and Fab fragments and recombinant single chain Fv in a human tumor xenograft model. Tumor Target 1996;2:37–48.
10. Wu AM, Chen W, Raubitschek A, et al. Tumor localization of anti-CEA single-chain Fvs: improved targeting by non-covalent dimers. Immunotechnology 1996;2:21–36.
11. Yokota T, Milenic DE, Whitlow M, Schlom J. Rapid tumor penetration of a single-chain Fv and comparison with other immunoglobulin forms. Cancer Res 1992;52:3402–8.
12. Mach JP, Pelegrin A, Buchegger F. Imaging and therapy with monoclonal antibodies in non-hematopoietic tumors. Curr Opin Immunol 1991;3:685–93.
13. Reilly RM, Sandhu J, Alvarez-Diez TM, Gallinger S, Kirsh J, Stern H. Problems of delivery of monoclonal antibodies. Pharmaceutical and pharmacokinetic solutions. Clin Pharmacokinet 1995;28:126–42.
14. Stehle G, Sinn H, Wunder A, et al. Plasma protein (albumin) catabolism by the tumor itself—implications for tumor metabolism and genesis of cachexia. Crit Rev Oncol Hematol 1997;26:77–100.
15. Wunder A, Stehle G, Sinn H, et al. Enhanced albumin uptake by rat tumors. Int J Oncol 1997;11:497–507.
16. Burger AM, Hartung G, Stehle G, Sinn H, Fiebig HH. Pre-clinical evaluation of a methotrexate-albumin conjugate (MTX-HSA) in human tumor xenografts *in vivo*. Int J Cancer 2001;92:718–24.
17. Kratz F, Muller-Driver R, Hofmann I, Drevs J, Unger C. A novel macromolecular prodrug concept exploiting endogenous serum albumin as a drug carrier for cancer chemotherapy. J Med Chem 2000;43:1253–6.
18. Wosikowski K, Biedermann E, Rattel B, et al. *In vitro* and *in vivo* antitumor activity of methotrexate conjugated to human serum albumin in human cancer cells. Clin Cancer Res 2003;9:1917–26.
19. Dennis MS, Zhang M, Meng YG, et al. Albumin binding as a general strategy for improving the pharmacokinetics of proteins. J Biol Chem 2002;277:35035–43.
20. Nguyen A, Reyes AE II, Zhang M, et al. The pharmacokinetics of an albumin binding Fab (AB.Fab) can be modulated as a function of affinity for albumin. Protein Eng Des Sel 2006;19:291–7.
21. Slamon DJ, Leyland-Jones B, Shak S, et al. Use of chemotherapy plus a monoclonal antibody against Her2 for metastatic breast cancer that overexpresses Her2. N Engl J Med 2001;344:783–92.
22. Carter P, Presta LG, Gorman CM, et al. Humanization of an anti-p185HER2 antibody for human cancer therapy. Proc Natl Acad Sci U S A 1992;89:4285.
23. Kelley RF, O'Connell MP, Carter P, et al. Antigen binding thermodynamics and antiproliferative effects of chimeric and humanized anti-p185HER2 antibody fragments. Biochemistry 1992;31:5434–41.
24. Leunig M, Yuan F, Menger MD, et al. Angiogenesis, microvascular architecture, microhemodynamics, and interstitial fluid pressure during early growth of human adenocarcinoma LS174T in SCID mice. Cancer Res 1992;52:6553–60.
25. Carter P, Kelley RF, Rodrigues ML, et al. High level *Escherichia coli* expression and production of a bivalent humanized antibody fragment. Bio/Technology 1992;10:163–7.
26. Finkle D, Quan ZR, Asghari V, et al. HER2-targeted therapy reduces incidence and progression of midlife mammary tumors in female murine mammary tumor virus huHER2-transgenic mice. Clin Cancer Res 2004;10:2499–511.
27. Jain RK. Understanding barriers to drug delivery: high resolution *in vivo* imaging is key. Clin Cancer Res 1999;5:1605–6.
28. Austin CD, De Maziere AM, Pisacane PI, et al. Endocytosis and sorting or ErbB2 and the site of action of cancer therapeutics Trastuzumab and Geldanamycin. Mol Biol Cell 2004;15:5268–82.
29. Hendriks BS, Wiley HS, Lauffenburger D. HER2-mediated effects on EGFR endosomal sorting: Analysis of biophysical mechanisms. Biophys J 2003;85:2732–45.
30. Colcher D, Pavlinkova G, Beresford G, Booth BJM, Choudhury A, Batra SK. Pharmacokinetics and biodistribution of genetically-engineered antibodies. Q J Nucl Med 1999;42:225–41.
31. Pavlinkova G, Beresford GW, Booth BJM, Batra SK, Colcher D. Pharmacokinetics and biodistribution of engineered single-chain antibody constructs of MAb CC49 in colon carcinoma xenografts. J Nucl Med 1999;40:1536–46.
32. Smith-Jones PM, Solit DB, Akhurst T, Afoze F, Rosen N, Larson SM. Imaging the pharmacodynamics of HER2 degradation in response to Hsp90 inhibitors. Nat Biotechnol 2004;22:701–6.
33. Williams LE, Wu AM, Yazaki PJ, et al. Numerical selection of optimal tumor imaging agents with application to engineered antibodies. Cancer Biother Radiopharm 2001;16:25–35.
34. Verhaar MJ, Chester KA, Keep PA, et al. A single chain Fv derived from a filamentous phage library has distinct tumor targeting advantages over one derived from a hybridoma. Int J Cancer 1995;61:497–501.
35. Kobayashi H, Shirakawa K, Kawamoto S, et al. Rapid accumulation and internalization of radiolabeled Herceptin in an inflammatory breast cancer xenograft with vasculogenic mimicry predicted by the contrast-enhanced dynamic MRI with the macromolecular contrast agent G6-(1B4M-Gd)256. Cancer Res 2002;62:860–6.
36. Tsai SW, Sun YY, Williams LE, Raubitschek AA, Wu AM, Shively JE. Biodistribution and radioimmunotherapy of human breast cancer xenografts with radiometal-labeled DOTA conjugated anti-HER2/neu antibody 4D5. Bioconjug Chem 2000;11:327–34.
37. De Santes K, Slamon D, Anderson SK, et al. Radiolabeled antibody targeting of the HER2/neu oncoprotein. Cancer Res 1992;52:1916–23.
38. Tang Y, Wang J, Scollard DA, et al. Imaging of HER2/neu-positive BT-474 human breast cancer xenografts in athymic mice using ^{111}In-trastuzumab (Herceptin) Fab fragments. Nucl Med Biol 2005;32:51–8.
39. Lub-de Hooge MN, Kosterink JGW, Perik PJ, et al. Preclinical characterisation of ^{111}In-DTPA-trastuzumab. Br J Pharmacol 2004;143:99–106.
40. Sutherland R, Buchegger F, Schreyer M, Vacca A, Mach J-P. Penetration and binding of radiolabeled anti-carcinoembryonic antigen monoclonal antibodies and their antigen binding fragments in human colon multicellular tumor spheroids. Cancer Res 1987;47:1627–33.
41. Krol A, Maresca J, Dewhirst MW, Yuan F. Available volume fraction of macromolecules in the extravascular space of a fibrosarcoma: implications for drug delivery. Cancer Res 1999;59:4136–41.
42. Sparreboom A, Scripture CD, Trieu V, et al. Comparative preclinical and clinical pharmacokinetics of a cremophor-free, nanoparticle albumin-bound paclitaxel (ABI-007) and paclitaxel formulated in Cremophor (Taxol). Clin Cancer Res 2005;11:4136–43.
43. Chaudhury C, Mehnaz S, Robinson JM, et al. The major histocompatibility complex-related Fc receptor for IgG (FcRn) binds albumin and prolongs its lifespan. J Exp Med 2003;197:315–22.
44. Minshall RD, Tiruppathi C, Vogel SM, Malik AB. Vesicle formation and trafficking in endothelial cells and regulation of endothelial barrier function. Histochem Cell Biol 2002;117:105–12.
45. Schnitzer JE, Oh P. Antibodies to SPARC inhibit albumin binding to SPARC, gp60 and microvascular endothelium. Am J Physiol 1992;263:H1872–9.
46. Tiruppathi C, Naqvi T, Wu Y, Vogel SM, Minshall RD, Malik AB. Albumin mediates the transcytosis of myeloperoxidase by means of caveolae in endothelial cells. Proc Natl Acad Sci U S A 2004;101:7699–704.